Biocompatibility of a Lab-on-a-Pill Sensor in Artificial Gastrointestinal Environments

Erik A. Johannessen, Lei Wang, Cathy Wyse, David R. S. Cumming, *Member, IEEE*, and Jon M. Cooper*

***Abstract*—In this paper, we present a radiotelemetry sensor, designed as a lab-in-a-pill, which incorporates a two-channel microfabricated sensor platform for real-time measurements of temperature and pH. These two parameters have potential application for use in remote biological sensing (for example they may be used as markers that reflect the physiological environment or as indicators for disease, within the gastrointestinal tract). We have investigated the effects of biofouling on these sensors, by exploring their response time and sensitivity in a model *in vitro* gastrointestinal system. The artificial gastric and intestinal solutions used represent a model both for fasting, as well as for the ingestion of food and subsequent digestion to gastrointestinal chyme. The results showed a decrease in pH sensitivity after exposure of the sensors for 3 h. The response time also increased from an initial measurement time of 10 s in pure GI juice, to ca. 25 s following the ingestion of food and 80 s in simulated chyme. These *in vitro* results indicate that changes in viscosity in our model gastrointestinal system had a pronounced effect on the unmodified sensor.**

***Index Terms*—Biofouling, *in vitro* measurements, lab-in-a-pill, microfabricated sensors, radio telemetry.**

I. Introduction

THE human gastrointestinal (GI) tract is relatively inaccessible to being probed with diagnostic sensors. This has resulted in a restricted knowledge of the causes, diagnosis and treatment of many GI diseases. Two important physico-chemical parameters that can provide useful information in clinical management of disease within the gut are those of temperature and pH. For example, GI temperature is not only a good indicator for the body core temperature [1], but local changes have also been shown to be associated with ulcers and tissue inflammation [2]. Likewise, pH can be used to identify pathological states associated with abnormal pH levels from the oesophagus to the distal colon, particularly those associated with pancreatic disease [3], portal hypertension [4], cystic fibrosis [5] and inflammatory bowel disease [6]–[9] as well as conditions involving gut interaction with host bacteria [10], [11]. In this latter respect, the activity of the predominant anaerobic flora alters the pH at the distal part of the GI tract, and it is therefore believed that this can be used as a diagnostic marker in assessing the function of the microbial population [12], [13]. Changes in local pH have also been shown to be associated with irritable bowel syndrome, rheumatoid arthritis [14], ankylosing spondylitis [15] and allergic airway disease [16].

The sensitivity and reproducibility of the diagnostic sensors will have a direct effect on their efficacy, and consequently on their ability to assess disease conditions. Measurements performed in biological environments, including those in the GI tract, will always be accompanied by effects associated with biofouling. To date, the majority of data on the biofouling of sensors have traditionally been studied in environmental monitoring of wastewater [17], marine environments [18], and implantations *in vivo* [19], with much less data available from measurements associated with the gut.

In this paper we present a novel telemetry sensor, designed as a lab-in-a-pill (LIAP), incorporating a dual channel microfabricated sensor and a custom made application specific integrated circuit (ASIC). The device was designed to enable non-invasive assessment of temperature and pH in the entire gut, and as a consequence, the ASIC included a power saving feature for extended service lifetime. The sensor platform was developed using standard CMOS and microfabrication technologies [20]–[22].

In this paper, the effects of biofouling are studied in three different model gastrointestinal systems *in vitro* and data concerning the response time and sensitivity are presented. In detail, these involved (i) artificial gastric and intestinal juice as a model for fasting; (ii) in a simulated environment concomitant with the ingestion of food; (iii) in gastrointestinal chyme. Sensor lifetime was monitored during the lifetime of the LIAP in order to assess detrimental effects on the device associated with prolonged exposure to GI solutions. All studies were restricted to the pH sensor alone, as the temperature sensor was embedded in the chip, and was not in direct contact with the test solutions.

II. Design and Fabrication

A. Sensors

The sensors were based on a research product with predefined n-channels in a p-type bulk silicon substrate from Ecole Superieure D'Ingenieurs en Electrotechnique et Electronique (ESIEE, France) which were modified by post lithographic pattern integration, described in more detail in prior publications [20]. The sensor chip comprised two separate parts, one acting as a pH ISFET with a microfabricated $Ag|AgCl$ reference electrode; the second as a temperature sensor (the n-channel of the

Manuscript received June 6, 2005; revised April 23, 2006. This work was supported in part by the Scottish Higher Education Funding Council under Grant RDG 130. *Asterisk indicates corresponding author.*.

E. A. Johannessen is with Lifecare AS, P.O. Box 1077, 3194 Horten, Norway (e-mail: erik.johannessen@lifecare.no).

L. Wang and D. R. S. Cumming are with the Department of Electronics and Electrical Engineering, University of Glasgow, Glasgow G12 8LT, UK.

C. Wyse is with the Department of Veterinary Clinical Studies, University of Glasgow, Institute of Comparative Medicine, Veterinary School, Glasgow G61 1QH, U.K.

*J. M. Cooper is with the Department of Electronics and Electrical Engineering, University of Glasgow, Glasgow G12 8LT, U.K. (e-mail: jmcooper@elec.gla.ac.uk).

Digital Object Identifier 10.1109/TBME.2006.883698

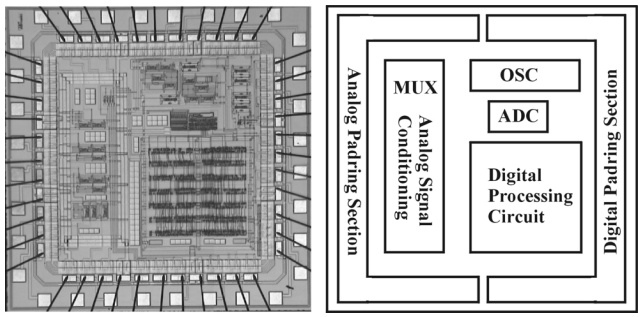

Fig. 1. Layout plot of the $4.5 \times 4.5\ \mathrm{mm}^2$ application specific integrated circuit control chip (left), and the associated explanatory diagram (right). MUX ADC, and OSC (32-kHz oscillator). The large bonding pads allow repetitive use of wire bonding for test and verification prior to integration in the LIAP.

second part comprised the silicon diode temperature sensor). The whole chip was subsequently encapsulated by a 50-μm -thick layer of polyimide (Durimide 7020, Arch Semiconductor, Belgium) with a window enabling direct access to the pH sensor without the use of dialysis membranes for improved response time. The dynamic range of the ISFET was tuned such that it could respond with a range from pH 1 to 10, with a temperature (reference) range from 10 °C to 50 °C.

B. ASIC

The ASIC control unit (Fig. 1) was designed using conventional EDA tools and fabricated as a 44-pin 20.25 mm^2 silicon die using a 3-V, 2-poly, 3-metal 0.6-μm CMOS process by Austria Microsystems (AMS, Austria). A key advantage of using the AMS process is the availability of well-specified analogue and digital IP blocks, such as the analog-to-digital converters (ADCs), operational amplifiers and standard I/O cells used in this design. The three functional blocks were designed to minimize size and reduce power consumption. These comprised the sensor interface (a 6-op-amp design and a multiplexer), a timer (with on chip circuitry using a RC relaxation oscillator which clocked the system at 32 kHz), and a system scheduler. A finite state machine represented the core of the system scheduler, which, together with a 10-bit ADC and related digital logic allowed several tasks to be performed such as sensor cycling and sampling.

A sleep modus and a serial bitstream data compression algorithm were used to enhance the power saving features. The algorithm decided when it was necessary to start a transmission by comparing the most recent data with the previous data during every sample interval. If the difference between the data sets was below a predefined tolerance limit, currently ± 1 least significant bits (LSB), the scheduler did not make a transmission. The data was instead compressed and stored on to a local buffer until the difference between samples was more than the tolerance limit, or when the buffer were full [23]. The system would rest at idle between transmissions. Thus, when quiescent, the system would run at 30% of full power.

The digitized data were fed directly into a small "on-off-keying" (OOK) AM transmitter module running at the licence-free 433.92-MHz ISM band. The data implemented the Manchester code, which translated combined clock and data signals at a rate of 4 $\mathrm{Kb\ s}^{-1}$. The data transmission pad was designed to provide up to 8 mA of output current, and as such powered up the radio transmitter (which were normally turned off) when the data was transmitted from the ASIC.

C. Base Station

The base station was used to capture pH and temperature data through wireless communication from the pill. The base station comprised a wireless interface module, a process core module and a data presentation module. The data presentation was achieved with a portable PC (Toshiba, Japan), the process core through a DAQ type PCMCIA card (National Instruments, U.S.) and the wireless interface through a miniaturized AM receiver. In order to set up a simplex wireless communication link between the LIAP and the base station, a TX7433AM 434-MHz ISM-band ON-OFF-Keying transmitter (in the LIAP) and a RX7433AM small superheterodyne receiver pair were chosen with a fixed reception frequency of 433.92 MHz (RF Solutions, U.K.). All components were battery operated. The data processing module ran on a Matlab 6 (Mathworks, U.S.) routine.

D. Capsule

The LIAP was assembled on a 0.8-mm double-sided PCB forming the backbone with predefined copper tracks defining the power supply rails, contact points for the sensors and an integrated single loop antenna corresponding to 1/16 λ. A schematic of the system (Fig. 2) illustrates the different components. The sensor chip and the ASIC were connected to the front of the PCB board, whereas a magnet (for telemetry), and a 433.92 AM transmitter (RF Solutions, U.K.) were both connected to the opposing side. The 3-V power supply was generated from two SR48 $\mathrm{Ag_2O}$ battery cells (Radio Spares, U.K.) with a capacity of 75 mAh, controlled by a rear mounted 7-pin 0.8-mm pitch socket (Radio Spares, U.K.) from which the device was activated (this latter feature was used during *in vitro* testing). The two 1.5-V batteries enabled the use of three reference voltages: positive (1.5 V), virtual ground (0 V) and negative (-1.5 V), as was required by the ASIC. The sensors and the ASIC were connected by wire bonding, whereas the two batteries were attached to slots made in the PCB. The contact points from the batteries were "cold soldered" using conductive glue (Chemtronics, Kennesaw, GA), whereas the wires running from the batteries and the transmitter were tin soldered onto the PCB.

The tracks and wires were cast in high strength epoxy (Radio spares, U.K.) for protection against the encapsulation material, whereas an inverted 2-mm high polypropylene "cup" (made from the bottom part of a 250 μL centrifuge tube, VWR, U.K.) attached by 3140 silicone rubber (Dow corning, U.S.) formed a seal protecting the sensors. The silicone rubber also prevented de-lamination between the sensor chip and the encapsulation material. The assembled device was then placed in a mould of PTFE, for encapsulation by a low viscosity epoxy resin, Araldite 2020, (Vantigo AG, Switzerland), which took 48 h to cure to a hard chemically resistant transparent polymer. After encapsulation, drilling a 3-mm hole down to the plastic cup, which was then removed, exposed the sensors. The complete device measured 12 × 36 mm and weighted 8 g including the batteries.

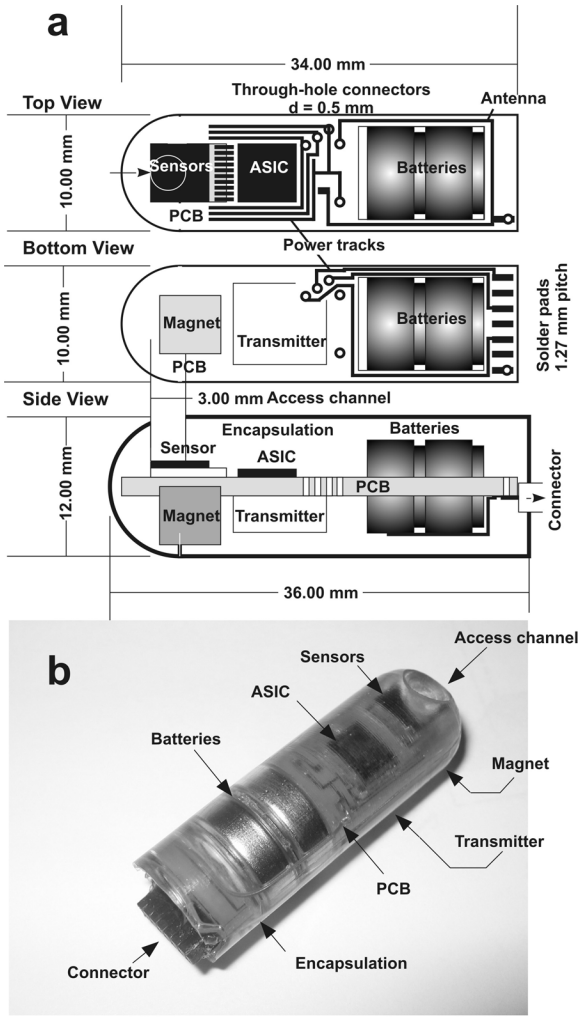

Fig. 2. Computer-aided design schematic illustrating the architecture of the LIAP. The sensor chip, incorporating a dual temperature and pH sensor, is located at the front, followed by the ASIC and batteries. The magnet and the transmitter are assembled on the reverse side. The whole unit is encapsulated in epoxy resin (Araldite 2020), with the external connector enabling powering both from the batteries and external sources.

III. Materials and Methods

The gastrointestinal environment is corrosive (low pH), with abundant bio-particles from proteins to carbohydrates and fat. Different *model* solutions representing the real gastrointestinal environment have previously been created *in vitro*.

Generally, the timescales over which processes associated with protein adsorption are of the order of minutes [19], and consequently measuring the effect of biofouling over periods of up to 3 h provided us with useful model data. The sensors were characterized using artificial made gastric and intestinal juice solutions as a model for fasting, with dissolved organic material (pet-food) as a model for the ingestion of food, and a high viscosity solution resembling the intestinal chyme.

A. Artificial Gastrointestinal Solutions

Gastric juice of pH 1.2 was made from 2 g sodium chloride (NaCl), 3.2 g pepsin (800 – 2500 iu mg^{-1}) and 7 mL 37 wt% hydrochloric acid (HCl) was made up to 1000 mL in reverse osmosis (RO) water. Likewise, the intestinal juice of pH 6.8 were made up from 6.8 g potassium phosphate – monobasic ($\mathrm{KH_2PO_4}$) dissolved in 250 mL RO water, 77 mL of 0.2 M sodium hydroxide (NaOH) and 10 g pancreatin made up to 1000 mL with RO water, and adjusted to pH 6.8 with 0.2 M HCl or 0.2 M NaOH. All chemicals and proteins were from Sigma Aldrich (U.K.).

Gastrointestinal solutions mixed in with 5% pet-food (Whiskas, U.K.) were used to represent partial digested food rich in fat, protein and solids (colloids). On addition of the pet-food, the pH of the gastric and the intestinal juice increased from pH 1.2 and pH 6.8 to pH 3.8 and pH 7.1, respectively.

The artificial chyme, which simulated digested food normally encountered in the stomach before the pill enters the small intestine, was identical to the gastric and intestinal juice, but with the water substituted with a milkshake solution (Friji, U.K.), containing 85% milk, skimmed milk powder, sugar, fat, cocoa powder, maize starch, stabilizers (carragenan, guar gum). The chemical composition of 100 mL gastric chyme was 0.2 g NaCl, 3.82 g protein, 11.7 g sugar, 1 g fat, 0.7 mL 37 wt.% HCl, and 117 mg calcium (Ca^{2+}), adjusted to pH 1.2. Likewise, 100 mL intestinal chyme contained 0.68 g $\mathrm{KH_2PO_4}$, 7.7 mL of 0.2 M NaOH, 4.5 g protein, 11.7 g sugar, 1 g fat and 117 mg Ca^{2+}, adjusted to pH 6.8.

B. A Model in Vitro Gastrointestinal System

All solutions were aliquoted in standard 25 mL universal tubes in which the LIAP telemetry device was immersed. An oscillating hot water bath (Grant, U.K.) simulated gastric peristalsis by moving the samples at 1 Hz while maintaining the temperature at 37 °C.

1) Calibration: The pH sensor was subject to a 4-point calibration routine at pH 1, 4, 7, and 10, both immediately before and after each experiment. Each calibration was repeated three times. The pill was immersed in each buffer solution for 2 min, with the data transmitted by wireless communication. The reading for each pH value was assigned corresponding datapoints. Similarly, the temperature sensor was also calibrated, by immersing the pill in a phosphate buffered saline (PBS) solution which was cooled to 8 °C and then heated to temperatures in the excess of 50 °C.

2) In Vitro Models: In the experimental protocols, the pill was first immersed in gastric juice for 45 min, and then directly transferred to intestinal juice to simulate the transition from the stomach (acidic environment) to the duodenum (neutral/alkaline environment) for another 45 min. Three repetitions were made of each 90-min run, for a total duration of 4.5 h. The protocol was then extended to involve a 60-min immersion in gastric chyme, before being transferred to intestinal chyme for another 60 min. The total duration of this run was 2 h.

IV. Results

The performance and technical data of the pill is summarized in Table I. The power consumption was 4.75 mW in the standby modus (3.9 mW attributed to the ASIC), whereas the power increased to 15.5 mW with the transmitter powered up for signal transmission. In our case, the transmission distance of the LIAP was maintained to 1 m from the receiving antenna and the signals from the sensors were recorded by the base-station with the

TABLE I
SUMMARY OF THE TECHNICAL DATA AND PERFORMANCE OF THE LIAP

Technical Data, LIAP		
Length x diameter:	36 x 12 mm	
Weight:	8.0 g, buoyancy less than water	
System controller:	Mixed signal ASIC, 0.6 μm CMOS, 3 metal/2poly	
Sensors/Type:	Ch 1: Temp (silicon diode) Ch 2: pH (ISFET)	
Dynamic range:	10 – 50 °C pH 1 - 10	
Sensitivity:	Temp 11.05 DP/°C pH 18.20 DP/pH unit	
Resolution:	Temp 0.25 °C pH 0.1	
Response time, temperature:	Buffer:	5.2 s
Response time, pH:	Buffer:	4.0 s
	Gastric/Intestinal Juice:	10 - 16 s
	Catfood solution:	13.8 - 24.0s
	Artificial Chyme:	~ 80.0 s
Transmission frequency:	433.92 MHz (SAW stabilised)	
Range:	~ 1 m	
Power source:	2 x SR48 Ag_2O, 3.1 volts, 75 mAh	
Power consumption ASIC	3.90 mW	
Power consumption LIAP:	4.65 mW (standby) ~ 15.5 mW (active)	
Service Lifetime:	< 42 hours (compress. ratio of 3.4)	
Capsule backbone:	PCB (power supply lines, antenna, signal out)	
Capsule skin:	2 component epoxy resin	

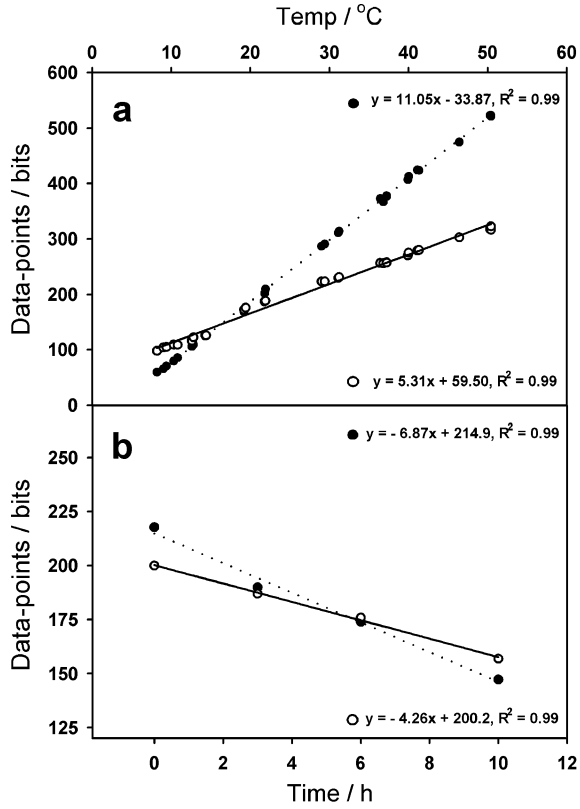

Fig. 3. Temperature sensitive responses (a) from both temperature (dotted line) and the pH channel (solid line) illustrating the inherent temperature dependency of any solid state semiconductor device. The battery supply voltage induced changes (b) were performed at 25 °C in a pH 7 buffer solution. The pH sensor was preconditioned in buffer for 24 h to cancel signal drift caused by the hydration of the proton sensitive membrane. The notation datapoints illustrate the RAW data acquired directly from the sensor prior to data processing.

data collected and presented in real time. All the characterization experiments were performed at 37 °C (body temperature).

A. Calibration

The calibration data from the temperature sensor showed a linear response throughout the dynamic range from 10 °C to 50 °C, Fig. 3(a). One degree temperature change (T) corresponds to 11.05 (~ 11) data-points ($f_T(T) = 11.05(T) - 33.9$, $\mathrm{R}^2 = 0.99$), indicating that the signal resolution of the temperature channel corresponds to 0.091 °C. However, it should be noted that the noise baseline corresponded to ± 2.5 bits (or $\pm 0.25\,^{\circ}\mathrm{C}$) such that, at 37 °C, the temperature reading corresponded to 375 ± 2.5 data-points. The response time (time factor $= \mathrm{V}_0 * \mathrm{e}^{-1}$) was measured to 5.2 s.

The signal from the temperature sensor could also be expected to change with the battery supply voltage [20], since the sensor biasing circuit and thus the diode current, I_D, was referenced to the negative supply voltage (-1.5 V). Thus, the signal change per hour (h) of 6.9 data-points h^{-1}, Fig. 3(b), ($f_{T\mathrm{supply}}(h) = -6.9(h) + 214.9$, $\mathrm{R}^2 = 0.99$) corresponds to a temperature fall of 0.62 °C h^{-1}. Given the temperature dependency of the pH sensor, it was decided that a compensation routine for this signal change could readily be implemented on chip, or later in the data processing algorithm.

The pH sensor exhibited a linear response from pH 1 to 10 (where one pH unit corresponded to 18.2 data-points ($f_{\mathrm{pH}}(\mathrm{pH}) = -18.2(\mathrm{pH}) + 328.9$, $\mathrm{R}^2 = 0.99$), Fig. 4. The resolution was determined to ± 0.1 pH by the inherent noise in the pH channel of the ASIC, and the response time in pure aqueous solutions measured to 4 s. Variations in the local

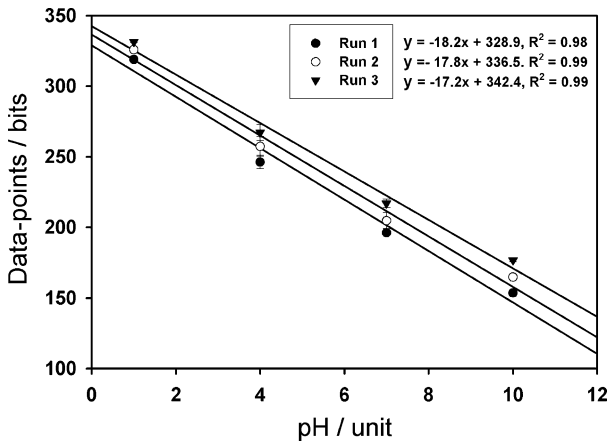

Fig. 4. Calibration chart of the pH sensor in gastric juice illustrating the positive increase in offset voltage due to hydration of the pH sensitive membrane, and the reduction in sensitivity as an effect of biofouling.

molar Cl^- concentration, [Cl^-], and its effect on the electrode potential was also explored by aliquoting KCl into the solution (at final concentrations of 0.01, 0.1, and 1.0 to 3 M). The linear regression analysis with [Cl^-] denoted by variable c, ($f_{\mathrm{REF}}(c) = 0.02(c) + 0.23$, $\mathrm{R}^2 = 0.91$) showed a sensitivity of 20 mV M^{-1} [Cl^-]. Since the expected change in [Cl^-] within the gut will not exceed 0.5 M, from pH 1 to pH 8, we can

conclude that resolution of the pH sensor with the integrated reference electrode should be approximate ± 0.2 pH units.

Being a semiconductor device, it was noted that the pH ISFET sensor responded to temperature in a similar manner to the silicon diode used for the temperature sensor [Fig. 3(a)]. The temperature response of the pH sensor ($f_{\mathrm{pH\,Temp}}(T) = 5.3(T) + 59.5$, $\mathrm{R}^2 = 0.99$) corresponded to 0.3 pH units per °C temperature change (considering a pH sensor response of 18.2 data-points pH^{-1}). Thus, the output signal from a pH 7 solution at 25 °C of 205 data-points, would be the equivalent of 270 data-points at 37 °C.

The pH sensor output also changed with the battery supply voltage [Fig. 3(b)] giving rise to a linear drift with time of -4.26 data-points h^{-1}, ($f_{\mathrm{pH\,supply}}(h) = -4.26(h) + 200.2$, $\mathrm{R}^2 = 0.99$). As a consequence, the temperature dependency resulted in a pH change of 3.6 from 25 °C to 37 °C, whereas the supply voltage induced a pH change of 0.23 units h^{-1}. Thus, it is clear that both temperature and supply voltage drift compensation of the pH channel will be required in future iterations of the device, to enable accurate measurements (this could either be implemented on chip through a voltage regulator, or as in this case, the data processing algorithm in the base station).

B. In Vitro Sensor Characterisation

1) Artificial Gastrointestinal Juice: The three calibration runs (Fig. 4) were performed prior to (run 1), after 90 min (run 2) and after 180 min (run 3) immersion in a gastrointestinal juice solution. The average sensitivity (measured by recalibrating the sensor between the runs) over the measured pH range decreased by 2.2% between run 1 and 2, and decreased by 5.5% between run 1 and 3. In contrast, the positive offset recorded in the trace increased from 328.9 to 336.5 and 342.4 data-points respectively. The error bars corresponds to ± 1 data-point, pH 1, (equiv. ± 0.06 pH) to ± 6.9 data-points, pH 4, (equiv. ± 0.38 pH) over the 20-min duration of the calibration protocol. The slow baseline drift with time that was observed after comparing the initial calibration (prior to run 1), with the calibration after 90 min (run 2) and 180 min (run 3), resulted in errors corresponding to ± 6.3 data-points, pH 1, (equiv. 0.35 pH) to ± 12.15 data-points, pH 10, (equiv. ± 0.67 pH).

The experimental results (Fig. 5) showed that the sensors did respond to changing pH throughout the experiment and did recalibrate after each 90-min run. On average the response time of the pH channel was measured to ca. 10 s in both the gastric and intestinal juice (after run 1), whereas the response time after run 2 had increased to 11.5 s in the gastric juice and 16 s in the intestinal juice. The recorded pH was 1.18 and 6.75 in the gastric and intestinal juice (run 1), and 1.26 and 6. 45 in the gastric and intestinal juice of run 2.

2) Ingested Meal: Tests conducted in artificially made gastric and intestinal juice mixed with pet-food (Fig. 6) showed that the sensors responded to a changing pH in the two solutions, and did recalibrate after each 90-min run. As seen with pure gastric and intestinal juice, the sensitivity was higher before than after the experiment. The measured values of the gastric and intestinal solution was 3.75 and 7.3 respectively in run 1, and 3.83 and 7.1 in run 2. The decrease in sensitivity was 1.15% between

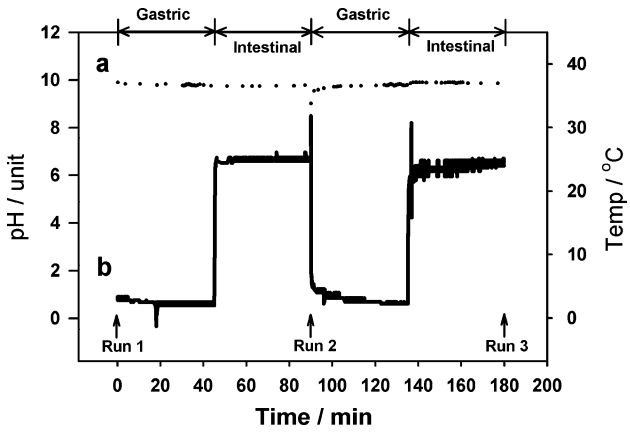

Fig. 5. Fasting model. Pill exposed to 180-min gastric (pH 1.2) and intestinal (pH 6.8) juice solution, presented with temperature (a) and pH channel. (b) Arrows indicate calibration runs of the pH sensor.

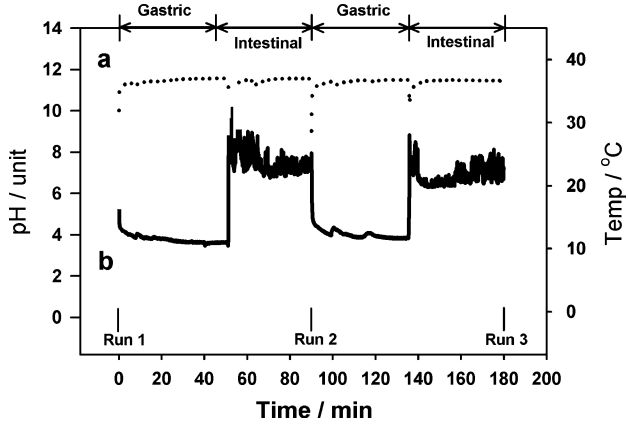

Fig. 6. Ingested meal model. Test sensor was exposed to 180-min artificial gastric juice (pH 3.8) and intestinal juice (pH 7.1) mixed with catfood. (a) The temperature and (b) the pH channel is shown. The sensor was calibrated prior to the measurement (t = 0), and after 90 and 180 min.

calibration run 1 and 2, and a further 2.8% in calibration run 3, was consistent with the trend observed for measurements in pure gastric and intestinal juice. The pH values obtained from the noisy readings of the intestinal juice were averaged over the previous 10 min. The response time from immersion in gastric juice was 13.8 s (run 1) and 24 s (run 2). The noise masked any measurements of the response time in the intestinal juice solutions.

3) Artificial Chyme: Recalibrating the sensors after the tests conducted in the artificial chyme showed that the sensitivity had been reduced by 3.85% to 17.5 data-points pH^{-1} after the 180-min run. Furthermore the response time of the pH sensor were now 80 s, clearly demonstrating the significance of performing measurements in more viscous solutions.

C. Longevity Tests

The pill was tested in the artificial gastrointestinal juice solution over three separate runs totalling 42 h running on battery power alone (Fig. 7). As expected, after prolonged usage, the offset voltage of the pH channel showed a decrease with time, which could be attributed to the falling supply voltage from the batteries (the pH sensor output is referenced to the positive

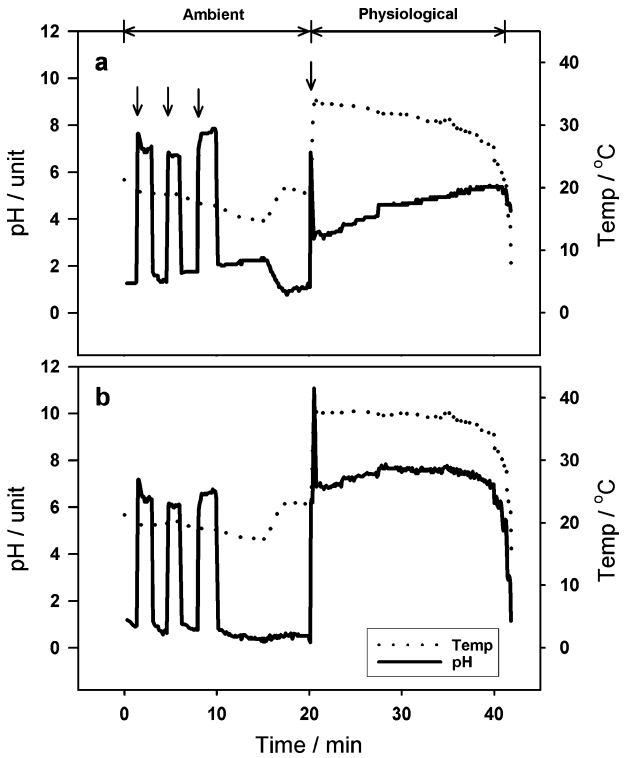

Fig. 7. Longevity tests and implementation of algorithm. (a) Raw data converted to pH (solid line) and temperature (dotted line). Three repetitive measurements were made in gastric and intestinal juice solutions (arrows), then immersion over night in gastric juice, before heating to 37 °C in intestinal juice until batteries were exhausted. Implementation of algorithm (b) zeroing out signal drift in the temperature channel (voltage) and both voltage and temperature drift in the pH channel. The algorithm provides comprehensive data, which are only compromised by nonlinear characteristics when the batteries are close to exhaustion.

supply rail, VSSA, [20]). The results Fig. 7(a) show temperature (dotted line) and pH (solid line). Throughout this period, the pill was successively immersed between gastric and intestinal juice (3 parallels) before resting in gastric juice until 20 h had passed. The pill was then immersed in intestinal juice at 37 °C for a further 22 h. At a constant temperature of 37 °C, one could clearly see the steady state drift in both sensor channels due to the reduced supply voltage from the batteries. The experiment continued until the batteries were exhausted. Thus, one can conclude that the SR48 Ag_2O batteries used were able to power the pill for up to 42 h in total.

It is clear that the influence of the battery supply voltage on the temperature channel, and the influence of both supply voltage and temperature on the pH channel, affects the performance of the system. Thus, an algorithm, based on the supply voltage characteristics of the temperature channel, and the supply voltage and temperature characteristics of the pH channel, was employed in the base-station side to offset these effects. The results Fig. 7(b) clearly illustrate how the temperature change between 16 and 20 h did not affected the pH sensor, which at the same time measured the correct pH readings from immersion in the gastric and intestinal juice. The drift in the temperature channel was significantly reduced, although the algorithm did not compensate for the non-linear characteristics seen in the circuitry due to failing batteries towards the end of the experiment.

V. Discussion

The change in offset voltage with time of the pH sensors can be explained by the hydration of the pH sensitive Si_3N_4 membrane changing the threshold potential, V_{th}, of the ISFET. The long-term signal drift (apparent in the intestinal juice solution) is believed to be a result from the interaction of proton reactive sites in the bulk of the Si_3N_4 membrane [24], with the drift becoming more predominant in alkaline solutions and at higher temperatures [25].

A. Artificial Gastrointestinal Juice

When compared to run 1, the delayed response from the pH sensor can clearly be seen in run 2 upon immersion in both gastric and intestinal juice. This effect can be attributed to biofouling, since the sensors, after recalibration, showed a reduced sensitivity. The source of biofouling was most likely absorption of pepsin and pancreatin on the pH sensitive membrane since this was the only organic agent present in both the gastric and intestinal juice. The consequence from the absorption of these proteins is that of either reducing the effective surface area of the sensor on which the protons can absorb to (lowering the sensitivity) or of generating an additional diffusion barrier through which the protons much pass (increasing response time). Both effects are apparent in Run 2.

In the gastric juice, the response time increased to 11.5 s (from 10.0 s), whereas the pH reading were 0.1 units above the recorded data from the previous run. The consequent immersion in the intestinal juice showed that the response time had now increased to 16 s, whereas the pH reading never came closer than 0.3 units below the recorded value from the previous run. One can therefore conclude the presence of biofouling in terms of reduced sensitivity and increased response time, although the function of the pH sensor was not significantly affected by this parameter.

B. Ingested Meal

The noisy recordings registered in the intestinal juice with partial digested pet-food were believed to be an effect of large particles (note that the sensor behaved normally upon recalibration). These particles could have generated noise by coming into contact with the pH sensitive gate membrane in the stirred solution (in the gastric juice, these particles were not visible due to the action of pepsin).

The observed temperature changes were a result from fluctuations due to the sensor moving in the more viscous solution. Corresponding fluctuations in the pH sensor were also apparent (Fig. 6 shows the raw data without implementation of the temperature compensation algorithm). The increased response time of the pH sensor of 13.8 s in run 1 and 24 s in run 2, reflected the increase in solution viscosity, but also the addition of secondary fouling agents such as dissolved fat or fatty acids present in the pet-food. The calibration data after removal of the sensors exhibited a similar response as observed for the pure gastric and intestinal juice experiments, thus any detrimental permanent effects from biofouling were considered as small.

C. Chyme

The main change in characteristic associated with measurements performed in the artificial chyme was the increased response time of the sensor to 80 s compared to the measurements from pure GI juice or juice mixed with pet-food. The increased viscosity of the solution provided a residual layer on the surface of the sensor, through which analyte has to diffuse. Cleaning the sensors removed this residual layer and subsequent recalibration showed that the response time were comparable to that in pure aqueous solutions (~ 4 s). Thus, allowances had to be made for a comparable delay in the real *in vivo* experiments. Considering an average passage speed of 0.3 $\mathrm{mm\ s^{-1}}$ in the small intestine [26], the capsule would have travelled 28 mm down the intestinal tract before the sensor would respond to the signal. Thus, a careful redesign by positioning the sensor much closer to the capsule surface could improve the response time in viscous solutions.

VI. Conclusion

Results showed that the sensitivity of the pH channel decreased between 3.8% and 5.5% during measurements of up to 180 min. The response time of the sensor increased from an initial 10 s in pure GI juice to 11.5 s in pure gastric juice and 16 s in pure intestinal juice respectively. Exposure to GI solutions mixed with 5% food increased the time from 13.8 s to 24 s, whereas the response time was measured to 80 s in simulated chyme. The *in vitro* results suggest that the biofouling on naked solid state silicon sensors did not significantly affect the data over the 3-h controlled measurement periods, and that the sensors would operate for a 42-h lifetime of the device. The data acquired with the increasing viscosity of the solutions, showed that measurements performed synchronous with the ingestion of food could be affected by the increased response time. In context, considering the slow passage speed in the gut, signals could still be detected within an accuracy of 30 mm in the small intestine. Thus, the potential of radiotelemetric chemical imaging would allow for screening of disease conditions without the requirement of visual aids.

Acknowledgment

The authors acknowledge technical staff at the University of Glasgow for the assistance in silicon microfabrication and the design of instrumentation. The authors further acknowledge H. Ward and C. Watt from the Veterinary School at the University of Glasgow for experimental support.

References

[1] I. B. Mekjavic, F. S. C. Golden, M. Eglin, and M. J. Tipton, "Thermal status of saturation divers during operational dives in the north sea," *Undersea Hyperbaric Med.*, vol. 28, pp. 149–155, 2001.

[2] R. T. Kung, B. Ochs, and J. M. Goodson, "Temperature as a periodontal diagnostic," *J. Clin. Periodontol.*, vol. 17, pp. 557–563, 1990.

[3] G. C. Kovacs, J. Furesz, L. Feketel, Z. Zaborszky, G. Orgovan, E. Kollar, and J. Regoly-Merei, "Calculated gastric intramucusal pH changes in the early phase of acute pancreatitis," *Orv. Hetil.*, vol. 140, pp. 941–945, 1999.

[4] D. Lamarque, D. Levoir, C. Duvoux, R. Herigault, C. Dutreuil, S. Adnot, D. Dhumeaux, and J. C. Delchier, "Measurement of gastric intramucosal pH in patients with circular and portal hypertensive gastropathy," *Gastroenterol Clin. Biol.*, vol. 18, pp. 969–974, 1994.

[5] M. Barraclough and C. J. Taylor, "Twenty-four hour ambulatory gastric and duodenal pH profile in cystic fibrosis: Effect of duodenal hyperacidity on pancreatic function and fat absorption," *J. Pediatr. Gastroenterol. Nutr.*, vol. 23, pp. 45–50, 1996.

[6] A. G. Press, I. A. Hauptmann, L. Hauptmann, B. Fuchs, K. Ewe, and G. Ramadori, "Gastrointestinal pH profiles in patients with inflammatory bowel disease," *Alimentary Pharmacol. Ther.*, vol. 12, pp. 673–678, 1998.

[7] K. Ewe, S. Schwartz, S. Petersen, and A. Press, "Inflammation does not decrease intralumminal pH in chronic inflammatory bowel disease," *Digestive Diseases Sci.*, vol. 44, pp. 1434–1439, 1999.

[8] P. Marteau, P. Lepage, I. Mangin, A. Suau, J. Dore, P. Pochart, and P. Seksik, "Review article: Gut flora and inflammatory bowel disease," *Aliment Pharmacol. Ther.*, vol. 20, pp. 18–23, 2004.

[9] D. Fish and S. Kugathasan, "Inflammatory bowel disease," *Adolescent Med. Clin.*, vol. 15, pp. 67–90, 2004.

[10] R. B. Sartor, "Therapeutic manipulation of the enteric microflora in inflammatory bowel disease: Antibiotics, probiotics, and prebiotics," *Gastroenterology*, vol. 126, pp. 1620–1633, 2004.

[11] Y. R. Mahida and V. E. Rolfe, "Host-bacterial interactions in inflammatory bowel disease," *Clin. Sci.*, vol. 107, pp. 331–341, 2004.

[12] R. A. Rastall, "Bacteria in the gut: Friends and foes and how to alter the balance," *J. Nutrition*, vol. 134, pp. 2022S–2026S, 2004.

[13] M. J. Farthing, "Bugs and the gut: An unstable marriage," *Best Pract. Res. Clin. Gastroenterol.*, vol. 18, pp. 233–239, 2004.

[14] B. N. Frizen, "Rheumatoid arthritis and the intestinal microbiocenosis," *Ter. Arkh.*, vol. 66, pp. 17–21, 1994.

[15] J. A. Hawrelak and S. P. Myers, "The causes of intestinal dysbiosis: A review," *Alternative Med. Rev.*, vol. 9, pp. 180–197, 2004.

[16] M. C. Noverr, R. M. Noggle, G. B. Toews, and G. B. Huffnagle, "Role of antibiotics and fungal microbiota in driving pulmonary allergic responses," *Infect. Immun.*, vol. 72, pp. 4996–5003, 2004.

[17] B. Q. Liao, D. M. Bagley, H. E. Kraemer, G. G. Leppard, and S. N. Liss, "A review of biofouling and its control in membrane separation bioreactors," *Water Environ. Res.*, vol. 75, pp. 425–436, 2004.

[18] B. B. Akhremitchev, J. E. Bernis, S. Al-Maawali, Y. J. Sun, L. Stebounova, and G. C. Walker, "Application of scanning force near field microscopies to the characterisation of minimally adhesive polymer surfaces," *Biofouling, suppl. S*, vol. 19, pp. 99–104, 2003.

[19] N. Wisniewski and M. Reichert, "Methods for reducing biosensor membrane biofouling," *Colloids Surfaces B: Biointerfaces*, vol. 18, pp. 197–219, 2000.

[20] E. A. Johannessen, L. Wang, L. Cui, T. B. Tang, M. Ahmadian, A. Astaras, S. W. Reid, P. S. Yam, A. F. Murray, B. W. Flynn, S. P. Beaumont, D. R. Cumming, and J. M. Cooper, "Implementation of multichannel sensors for remote biomedical measurements in a microsystems format," *IEEE Trans. Biomed. Eng.*, vol. 51, no. 3, pp. 525–535, Mar. 2004.

[21] T. B. Tang, E. A. Johannessen, L. Wang, A. Astaras, M. Ahmadian, A. F. Murray, J. M. Cooper, S. P. Beaumont, B. W. Flynn, and D. R. S. Cumming, "Toward a miniature wireless integrated multisensor microsystem for industrial and biomedical applications," *IEEE Sensors J.*, vol. 2, no. 6, pp. 628–35, Dec. 2002.

[22] L. Wang, E. A. Johannessen, P. Hammond, L. Cui, J. M. Cooper, S. W. J. Reid, and D. R. S. Cumming, "A programmable microsystem using system-on-chip for real-time biotelemetry," *IEEE Trans. Biomed. Eng.*, vol. 52, no. 7, pp. 1251–1260, Jul. 2005.

[23] L. Wang, T. B. Tang, E. A. Johannessen, A. Astaras, A. F. Murray, J. M. Cooper, S. P. Beaumont, and D. R. S. Cumming, "An integrated sensor microsystem for industrial and biomedical applications," presented at the IEEE Instrumentation and Measurement Technology Conf, Anchorage, AK, 2002.

[24] D. Yu, Y. D. Wei, and G. H. Wang, "Time-dependent response characteristics of pH-sensitive ISFETS," *Sens. Actuators B*, vol. 3, pp. 279–285, Apr. 1991.

[25] P. Hein and P. Egger, "Drift behaviour of ISFETS with Si3N4 – SiO2 gate insulator," *Sens. Actuators B*, vol. 13–14, pp. 655–656, 1993.

[26] L. Sherwood, *Human Physiology from Cells to Systems*, 2 ed. Minneapolis, MN: West, 1993, p. 745.

Erik A. Johannessen received the B.Sc. degree in natural sciences from the University of Tromsø, Tromsø, Norway, in 1997, and the Ph.D. degree from the University of Liverpool, Liverpool, U.K., in 2002. The Ph.D. project was funded by the Wellcome Trust focusing on the development of ultra-small nanocalorimetric sensors for integration in high-density assay screening of cells.

He has since worked as a Postdoctoral Researcher with the Department of Electronic and Electrical Engineering at the University of Glasgow, Glasgow, U.K., and is currently employed as project manager in Lifecare, Horten, Norway. His research interests focus on bio and nanoelectronics, MEMS and mobile analytical microsystems.

Lei Wang received the B.Sc. degree in information and control engineering and the Ph.D. degree in biomedical engineering from the Xi'an Jiaotong University, Xi'an, Shanghai, China, in 1995 and 2000 respectively.

He has worked as a Postdoctoral Researcher with the Department of Electronic and Electrical Engineering, the University of Glasgow, Glasgow, U.K, during 2001–2005. He is currently with the Department of Computing, Imperial College London, London, U.K. His research interests focus on biomedical signal processing, medical electronics, and IC design.

Cathy Wyse received the B.A. (Hons) degree in equine science from Coventry University, Coventry, U.K., in 1996, and the M.Sc. degree in veterinary science from the University of Glasgow, Glasgow, U.K., in 1999. The Ph.D. degree was awarded in 2003, following a collaborative project between the Division of Veterinary Clinical Studies, and the Division of Bioelectronics at the University of Glasgow.

She is currently working as a Research Associate at the University of Bristol, Bristol, U.K. Her research interests include the development of novel diagnostic methods in veterinary medicine, and on factors affecting performance in racehorses.

David R. S. Cumming (M'97) received the B.Eng. degree in electronic engineering from the University of Glasgow, Glasgow, U.K., 1989 and the Ph.D. degree from the University of Cambridge, Cambridge U.K., in 1993.

He is currently Professor of Microsystem Technology and EPSRC Advanced Research Fellow in Electronics and Electrical Engineering at the University of Glasgow where he leads the Microsystem Technology Group and Electronics Design Centre for Heterogeneous Systems. He has worked on mesoscopic device physics, RF characterization of novel devices, fabrication of diffractive optics for optical and sub-millimeter wave applications, diagnostic systems, and microelectronic design.

Jonathan M. Cooper received the B.Sc. degree in biological sciences from the University of Southampton, Southampton, U.K., in 1983 and the Ph.D. degree in sensor technology from the University of Cranfield, Bedfordshire, U.K., in 1989.

He is a Professor of Bioelectronics and Bioengineering in the Department of Electronic and Electrical Engineering at the University of Glasgow, Glasgow, U.K. His research interests lie in the areas of biosensors for clinical diagnostics, Lab-on-a-Chip technologies and Bionanotechnology. He was elected as a fellow of the Royal Society of Edinburgh and of the Royal Academy of Engineering.